Article

Development of a Comprehensive Approach to Quality Control of Dermorphin Derivative—Representative of Synthetic Opioid Peptides with Non-Narcotic Type of Analgesia

Vasilisa A. Sukhanova [1], Elena V. Uspenskaya [1,*], Safdari Ainaz [1], Hoang Thi Ngoc Quynh [1] and Aleksey A. Timofeev [2]

[1] Department of Pharmaceutical and Toxicological Chemistry, Medical Institute, Peoples' Friendship University of Russia Named After Patrice Lumumba (RUDN University), 6 Miklukho-Maklaya St., Moscow 117198, Russia; skhnv.vasilisa@gmail.com (V.A.S.); ainazsafdari98@gmail.com (S.A.); ngocquynhyk@gmail.com (H.T.N.Q.)

[2] Scientific and Educational Resource Centre "Innovative Technologies of Immunophenotyping, Digital Spatial Profiling and Ultrastructural Analysis", Peoples' Friendship University of Russia Named After Patrice Lumumba (RUDN University), 6 Miklukho-Maklaya St., Moscow 117198, Russia; alexpismo77@mail.ru

* Correspondence: uspenskaya75@mail.ru; Tel.: +7-916-655-79-86

Abstract: Peptides occupy a significant share of the pharmaceutical market and are among the top-200 selling drugs in the group of non-insulin drugs with analgesic, antibacterial and cardiovascular effects. The aim of this work is to develop a comprehensive analytical approach for quality control of novel synthetic peptides with non-narcotic types of analgesia and to provide docking simulations of dermorphin complex formation at the μ-opioid receptor (MOR) binding site. The materials and methods used include the pharmaceutical substance dermorphin tetrapeptide (DMTP) (tyrosyl-D-arginyl-phenylalanyl-glycinamide); Fourier transform infrared spectroscopy (FT-IR); static and dynamic laser light scattering (DLS, LALLS); scanning optical microscopy (SEM); X-ray fluorescence elements analysis; polarimetry for optical activity determining; and *Spirotox* method for sample biotesting. FT-IR-Spectra indicated specific amino acid chemical groups in the tetrapeptide sequence at 3300–2700 cm^{-1}, 1670 cm^{-1}. UV-absorption spectra of aqueous solutions of dermorphin tetrapeptide showed an absorption maximum at 275 nm, which is in good agreement with the presented spectrum of the bovine serum albumin (BSA) standard; the Pearson's r of calibration line "A-C%" in 0.0125% to 0.0500% concentration range is 0.999; and the calculated specific extinction value $E_{1cm}^{1\%}$ = 18.38 ± 0.23. Of the 11 elements detected by X-rays, the elements copper (Cu) and cobalt (Co) have the highest X-ray intensity. Dispersion characteristics of dermorphin solutions were studied in the submicron and micron range. Conglomerates and druzes were detected by SEM, ranging in size from 2 μm to 100 μm. The specific optical activity index was calculated $[\alpha]_D^{20}$ = +36.18 ± 2.04 [°·mL·g^{-1}·dm^{-1}], according to Biot's Law. Additionally, the orientation and conformation of the dermorphin molecule in the active binding site of the 8E0G receptor were predicted using molecular modeling, revealing that the contact area affects the key amino acid residue arginine (ARG 182). This comprehensive approach to analytical methods for qualitative and quantitative analysis of dermorphin tetrapeptide can be applied in pharmacies to enhance the understanding of its biological activity and aid in the development of regulatory documentation for a new, non-narcotic analgesic based on the dermorphin tetrapeptide.

Keywords: synthetic dermorphin tetrapeptide; non-narcotic analgesia type; quality control; physico-chemical analysis; molecular docking; *Spirotox* test

1. Introduction

Opioids have been used for thousands of years for the treatment of acute and chronic pain. They primarily act in the central nervous system, where they modify the ascending pain pathway. Opioids produce analgesia by binding to μ-opioid receptor (MOR) and modifying ion channel function. They reduce pain by inhibiting the influx of voltage-gated calcium channels into the presynaptic neuron, which is the primary afferent fiber, and subsequently preventing the release of neurotransmitters. Additionally, they increase the potassium conductance of second-order sensory neurons in the dorsal horn of the spinal cord. These effects make opioids some of the most powerful analgesic drugs, but their use requires careful consideration [1]. However, opioid analgesics are capable of causing serious side effects, such as severe forms of drug abuse and dependence [2,3]. The increase in opioid prescribing has led to a dramatic increase in opioid abuse, as well as the prevalence of complications such as overdose and death [4]. In the USA, in 2021, there were over 80,000 deaths related to opioids. The phenomenon of the rapid increase in non-prescription opioid use has been termed the "opioid crisis".

Dermorphin derivatives belong to a class of endogenous opioid peptides and are among the most potent analgesics known. Their high analgesic activity is due to the unique primary structure of these substances, which are the only eukaryotic regulatory peptides that contain a D-amino acid. In 1981, researchers isolated a peptide from the skin of South American frog species from the genus *Phyllomedusa* and named it dermorphin [5]. It has been revealed that substances derived from amphibians contain many bioactive compounds, including peptides that exert analgesic effects. Meanwhile, the genus *Phyllomedusa* represents an important source of peptides and biologically active components. Containing D-amino acids, peptide opioids are abundant in the skin secretions of *Phyllomedusa* [6]. It has been found that only the serous glands of amphibians specifically participate in the biosynthesis and secretion of bioactive substances (BAS) [7,8] (Figure 1).

(**a**)　　　　　　　　　　(**b**)
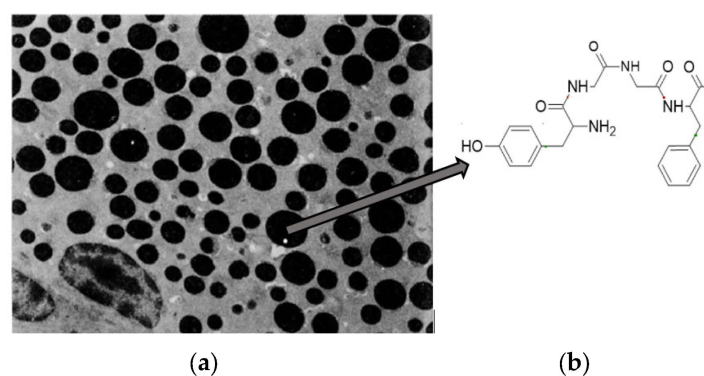
Figure 1. Microphotographs of a skin section of *Phyllomedusa sauvagii* taken with a transmission electron microscopy: (**a**) image of type Ia serous glands (in the inset—dissected spherical granules of secretion containing bioactive substances); (**b**) pharmacophores of aromatic amino acid residues in the structure of natural opioid peptides.

This discovery marked the start of a series of studies on both dermorphin and its natural analogs, which led to the discovery of an extensive family of peptides that are similar to dermorphin [9]. Dermorphin and its analogs may provide a new target molecule for developing novel analgesics that have higher intrinsic activity and fewer side effects than morphine [10].

An innovative tetrapeptide, H-Tyr-D-Arg-Phe-Gly-NH$_2$, which is a synthetic derivative of dermorphin tetrapeptide (DMTP), is claimed to be a highly promising candidate for the treatment of chronic pain [11]. It is now generally believed that the stimulation of μ1

receptors causes supraspinal analgesia, while the effects of μ2 receptors are responsible for the spinal analgesia and euphoria observed, as well as respiratory depression, mydriasis, and weakening of gastrointestinal motility [12].

H-Tyr-D-Arg-Phe-Gly-NH$_2$ is a highly selective agonist of the μ1-opioid receptor, with minimal interaction with other opioid receptors, which makes it a crucial difference in treating chronic pain in cancer patients. Based on the results of the clinical studies in phases I and II, a high analgesic efficacy for the drug DMTP was demonstrated, along with a more favorable safety profile compared to morphine [13].

However, a recent study [14] revealed that dermorphin positively modulates the homomeric acid-sensing ion channels (ASIC1α) and ASIC3, as well as the ASIC3-containing heteromeric channels. These channels, preferably having a neuronal localization, play an important role in the functioning of the central nervous system (CNS) and peripheral nervous system (PNS), positive modulation of which may cause possible side effects. It would be important to take this fact into consideration.

As for an innovative drug, the development of quality-control approaches using available methods, as well as an understanding of the mechanisms of interaction with cellular receptors, is particularly relevant.

The aim of the present work is to develop a combination of previously unused physic-ochemical analytical and in silico molecular docking techniques to characterize the dispersive, morphological, optical, spectral, chemical, and biological properties of the synthetic μ1-opioid receptor agonist dermorphin tetrapeptide with a non-narcotic type of analgesia.

2. Materials and Methods

2.1. Powder Substances

The object of the study is the pharmaceutical substance of dermorphin tetrapeptide (Tyrosyl-D-arginyl-phenylalanyl-glycinamide, C$_{26}$H$_{36}$N$_8$O$_5$, Mr = 540.6 produced by Sotex PharmFirm, Moscow, Russia) (Figure 2).

H-Tyr-Arg-Phe-Gly-NH$_2$
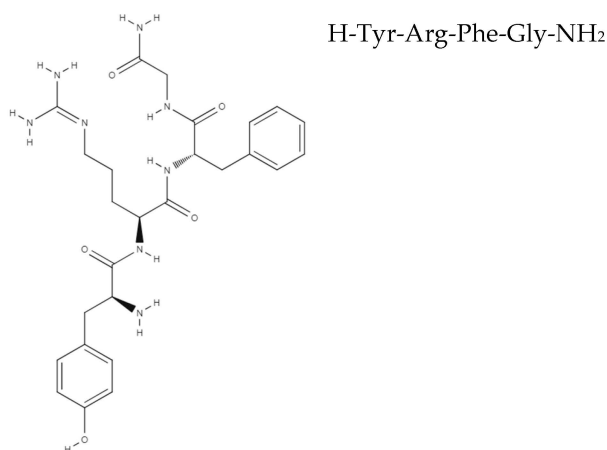
(2S)-2-[[(2S)-2-amino-3-(4-hydroxyphenyl)propanoyl]amino]-N-[(2S)-1-[(2-amino-2-ox-oethyl)amino]-1-oxo-3-phenylpropan-2-yl]-5-(diaminomethylideneamino)pentanamide

Figure 2. Dermorphin tetrapeptide structure and its IUPAC condensed [15].

Tyrosyl-D-arginyl-phenylalanyl-glycinamide is a white crystalline powder, which is hygroscopic and readily soluble in water (logP~1.7).

Bovine serum albumin (BSA) lyophilized (Santa Cruz Biotechnology, Inc., Dallas, TX, USA, CAS No: 9048-46-8, F.W.~66 kDa, 585 amino acid residues) was used as a standard for quantitative determination of polypeptide concentration by UV-spectroscopic method.

For this purpose, solutions of BSA in 0.9% NaCl with protein concentrations ranging from 0.2 mg/mL to 2.0 mg/mL were prepared.

2.2. Fourier Transform Infrared (FT-IR) Spectroscopy

The vibrational spectrum of the DMTP substance in the spectral range from 4000 to 400 cm^{-1} was obtained using an Agilent Cary 630 FT-IR spectrophotometer (Agilent, Santa Clara, CA, USA) with a resolution of 2 cm^{-1}, equipped with a diamond crystal attachment in Attenuated Total Reflectance (ATR) mode and basic software. Approximately 1 mg of the drug powder was placed on the measuring surface of the ATR attachment without prior sample preparation in order to obtain a spectrum of suitable intensity for further study.

2.3. Electron Spectroscopy

To obtain electronic absorption spectra of aqueous solutions with concentrations from 0.0125% to 0.0500% in the range from 200 nm to 350 nm, AGILENT Cary 60 equipment manufactured by Agilent in Santa Clara, CA, USA was used (T = 22.0 $\pm$ 0.5 °C).

2.4. Dynamic Light Scattering (DLS)

Dynamic light scattering from the ZetasizerNano ZSP instrument (Malvern Panalytical, Worcestershire, UK) was used to determine particle size in 0.25% aqueous DMTP solution in the range from 1 nm to 10,000 nm (T = 22.0 $\pm$ 0.5 °C).

2.5. Low-Angle Laser Light Scattering (LALLS)

Measurements of the DMTP particle size in the range of 0.1 microns to 180 microns were performed using a laser analyzer (Malvern Instruments, Malvern, UK) with a scanning wavelength of λ = 632 nm and a capacitive cell (V = 3 mL) equipped with a mechanical stirrer. The radiation scattered by the particles of the dispersed phase was recorded at different angles using a highly sensitive multi-element detector—a photodiode array. Sample preparation consisted of preparing a 0.01% DMTP dispersion in n-hexane (99.0% purity), which also served as a background sample for pre-recording. For each aliquot, three repeated measurements were made within 30 s, corresponding to 30,000 separate light scattering measurements.

2.6. Polarimetry

The optical activity of aqueous solutions of DMTP in the concentration range of 0.25% to 2.00% was analyzed using an Atago automatic polarimeter (model POL$-1/2$, JJS Technical Services, Chicago, IL, USA). Measurements were made in a 100 mm diameter cell with an accuracy of $\pm$ 0.002° and a resolution of 0.0001°, as well as a measured wavelength λ = 589 nm (D-line). The temperature was controlled at 20 °C using an electronic Peltier module. The optical angle of rotation was measured at *n* = 5 for a solution of each concentration. The results are presented both as α, °C, % linear dependence, and as the value of the specific optical rotation, depending on the nature of the substance.

2.7. X-Ray Fluorescence Analysis (XRF)

The elemental composition measurements were conducted using an energy-dispersive spectrometer EDX-7000P (Shimadzu Europa GmbH, Duisburg, North Rhine-Westphalia, Germany) based on a silicon drift detector with thermoelectric cooling, equipped with the PCEDX-Navi (No. 01-00300-EN) software package. The characteristic X-ray excitation in the sample was performed using an X-ray tube with a rhodium (Rh) anode, operating at a voltage of 50 kV and an electron current of 1–1000 µA; the irradiation area was controlled by a 10 mm collimator. The fluorescence X-rays from the samples were registered by a Peltier-cooled silicon drift detector. The range of elements measured by the X-ray fluorescence

method spanned from 11Na to 92U. The powdered sample of the pharmaceutical substance of dermorphin tetrapeptide was placed in a cuvette covered with a Mylar (polyester) film in an air atmosphere, positioned in the center of the instrument window, and measured.

Sample «NIST SRM 2976» manufactured at MEL IAEA (Marine Environment Laboratories of International Atomic Energy Agency, Monaco) and certified by the National Institute of Standards and Technology (NIST, Gaithersburg, MD, USA) was used as a standard reference material [16].

Determination of the content of a chemical element in the sample was conducted using the formula:

$$C_X = C_{st} \cdot \frac{I_X}{I_{st}}, \tag{1}$$

where C_X and C_{st}, I_X and I_{st} are the element concentration (μg/g) and fluorescence intensity (cps/mA) in the test ($_X$) and standard ($_{st}$) samples, respectively.

2.8. Spirotox Biotesting

The study of the biological activity/toxicity of dermorphin tetrapeptide was conducted using the *Spirostomum ambigua* test culture, characterized by statistically reliable sensitivity to toxicants. The kinetic scheme caused by ligand death of *S. ambigua* is described in [17] in detail. The dependence of test culture lifetime (t_L, s) on temperature (T, K) is linearized in "Arrhenius coordinates"

$$k = A \cdot e^{-\frac{E_a}{RT}}, \tag{2}$$

where k is the reaction rate constant, A is the pre-exponential multiplier characterizing the frequency of collisions of reacting molecules, e is the base of the natural logarithm, E_a is the activation energy, kJ/mol, R is the universal gas constant (8.31 J/mol $\cdot$ K), and T is the temperature, K.

Study Design

The study of the Arrhenius kinetics of the transition of a cellular biosensor to the immobilized state (*Spirotox*) included the stage of selecting the concentration of an aqueous solution of dermorphin tetrapeptide, based on the condition that t_L (s) = 60 $\div$ 1200 at T = 24.0 °C. It was found that in a 1% aqueous solution of DMTP, the cellular biosensor died instantly, whereas in a 0.01% aqueous solution, it survived for more than 30 min. Consequently, for the *Spirotox* study, a 0.1% aqueous solution (pH = 5.47 $\pm$ 0.01) was prepared. The temperature range was 24 °C to 32 °C in 2 °C increments (n = 6). The study results are presented in direct (t_L, s $-$ T, K) and Arrhenius (ln $1/t_L$ $-$ $1/T$) coordinates, from which the activation energy of the cell transitions to the DC (death cell) stage, overcoming the intermediate state, is calculated (Scheme 1).
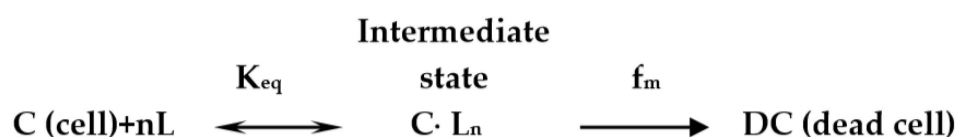
Scheme 1. Kinetic scheme of ligand–receptor interaction *S. ambigua* with low molecular ligand: C-cell, L-ligand, n-stoichiometric coefficient, C·L$_n$—intermediate state (cell after interaction with the ligand), K_{eq} is the equilibrium constant fast stage, f_m is the rate constant of the cell transition to the dead state, and DC is a dead cell.

2.9. Scanning Electron Microscopy (SEM)

The size, shape, and texture of the powdered specimens of the dermorphin tetrapeptide substance were characterized using a fourth-generation scanning electron microscope (SEM, LYRA 3, Tuscany, Brno-Kogoutovice, Czech Republic) with a Schottky cathode with a maximum resolution of 1 nm and a maximum magnification of 1,000,000 times, with pre-vacuuming of the samples and removal of excess charge from the surface by applying an amorphous carbon layer.

2.10. Molecular Docking

To conduct our docking study, we selected the high-resolution crystal structure of the active μ-opioid receptor (MOR) model, with a high resolution of 2.10 Å (PDB ID: 8E0G). This particular crystal structure provides detailed insights into the conformation of the receptor in its active state. In light of this observation, it was decided to focus the study the A-chain of the MOR. The A-chain sequence, sourced from the Mus musculus species, was selected as the target for our docking simulations. The preliminary preparation of the protein model involved removing solvent molecules, adding polar hydrogen atoms, and recovering missing atoms using the AutoDockTools 1.5.7 program [18]. Rosetta FlexPepDock server "http://flexpepdock.furmanlab.cs.huji.ac.il/" (accessed on 20 March 2024), whose working framework is peptide docking protocol, was applied to obtain the pose of Tyr-Arg-Phe-Gly (YRFG) with mu-type opioid receptor, as well as to calculate the function score to predict its favorable binding pose within the receptor's binding pocket [19]. The corresponding ab initio FlexPepDock version can fold a peptide within a binding site using a Rosetta fragment-based approach [20].

2.11. Statistical Analysis

All results obtained were analyzed using statistical methods as means $\pm$ standard deviation (SD) of different and independent experiments ($n \geq 3$) with the assistance of software packages provided by OriginPro 2021 9.80.200 (OriginLab Corporation, Northampton, MA, USA). p values < 0.05 were considered significant.

3. Results

3.1. Spectral Methods

For the analytical quality control of medicines containing DMTP, we have proposed modern pharmacopoeial methods, including the first and second approaches to identification.

This section presents the results of qualitative and quantitative analysis of the DMTP substance using spectroscopic methods.

3.1.1. FT-IR Spectroscopy Analysis

Extraction and identification of biologically active polypeptides from natural sources (plants, animals, insects), which are products of proteolysis, pose a nontrivial task [21–24]. This is due to the natural fragmentation of peptides, followed by defining the "peptidome" as the set of all fragments of the same substance [25]. Established biochemical approaches exist for the analysis of peptide fragments based on the combined use of electrophoresis and MALDI-TOF mass spectrometry [26]. However, approaches to peptide identification based on obtaining and analyzing bands, conditioned by vibrational transitions in the peptide score, allow for express identification. The vibrational–rotational spectrum of the DMTP was acquired using the FT-IR spectroscopy techniques shown in Figure 3.
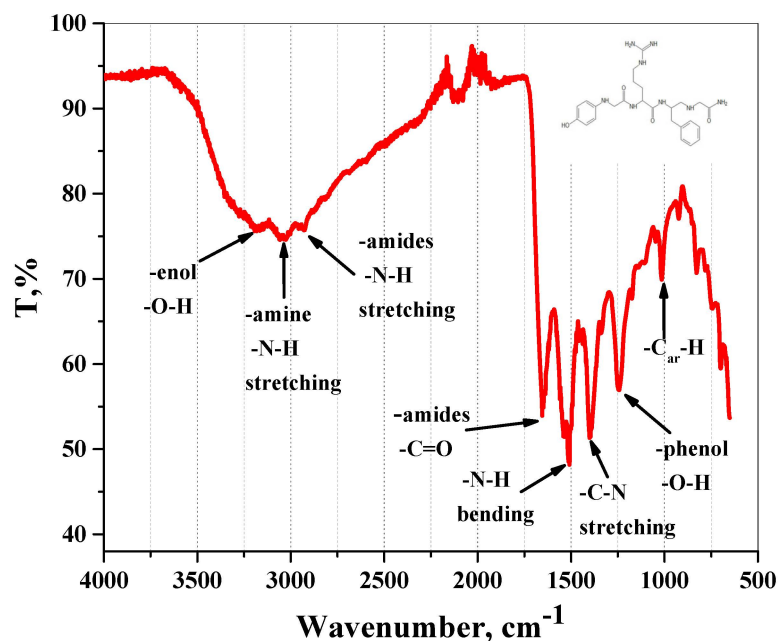
Figure 3. FT-IR spectrum of dermorphin tetrapeptide substance.

The wide light bandwidth in the high-frequency range of 3300–2700 cm^{-1} covers the -NH groups in the residues of aromatic, aliphatic amines, and imines, as well as the -OH groups, due to phenolic residue and also to lactam–lactim tautomerism in amino acid residues in the tetrapeptide due to the intramolecular proton transfer (IPT) process (Scheme 2).

Lactam (keton) form   **Lactim (enol) form**
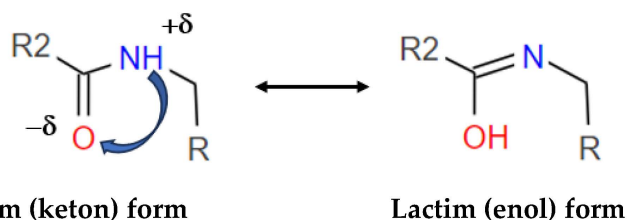
Scheme 2. Lactam–lactim type of dermorphin tetrapeptide's amide–imidol tautomerism. This type of tautomerism occurs when hydrogen shifts between nucleophilic oxygen and nitrogen of NH-acid center.

According to [27], the predominant tautomer at room temperature is the lactam form, while the enthalpy of the lactam–lactim transition is about 2–3 kJ/mol.

A band at 1670 cm^{-1} corresponds to fluctuations in the C=O bond in amides, while a band near 1390 cm^{-1} is attributed to fluctuations in bonds in methylene groups (-CH$_2$-) contained in tyrosine-arginine-phenylalanine-glycine amide residues, and a band at 1300 cm^{-1} corresponds to the -C-N group (Table 1).

**Table 1.** The transmittance bands in the dermorphin tetrapeptide FT-IR spectra.

Wavenumber, cm^{-1}	Chemical Group	Compound Class	Appearance
3700–3200	O-H stretching	Alcohol	Strong
3350–3310	N-H-stretching	Secondary amine	Medium

Table 1. *Cont.*

Wavenumber, cm^{-1}	Chemical Group	Compound Class	Appearance
near 3350 and 3180	N-H stretching	Primary amides	Strong
3300	N-H stretching	Secondary amides	Strong
1660	C=O stretching	Amide	Strong
1670–1640	C=N stretching	Imine (tautomer)	Medium
near 1500	N-H bending	Primary/secondary amides	Strong
1450–1375	C-H bending	Methyl group	Medium
near 1400	C-N stretching	Amide	Medium
1420–1330	O-H bending	Alcohol (tautomer)	Medium
1300	C-N stretching	Amine	Medium
near 1000	C-H stretching	Aromatic compound	Strong

3.1.2. Electron Spectroscopy Analysis

It is known that most α-amino acids hardly absorb electromagnetic radiation in the visible spectrum [28]. Those amino acids whose molecules contain aromatic and/or heterocyclic fragments are absorbed in the UV region, which was recorded by us when studying the absorption of aqueous DMTP solutions in the concentration range from 0.0125% to 0.0500% (Figure 4).
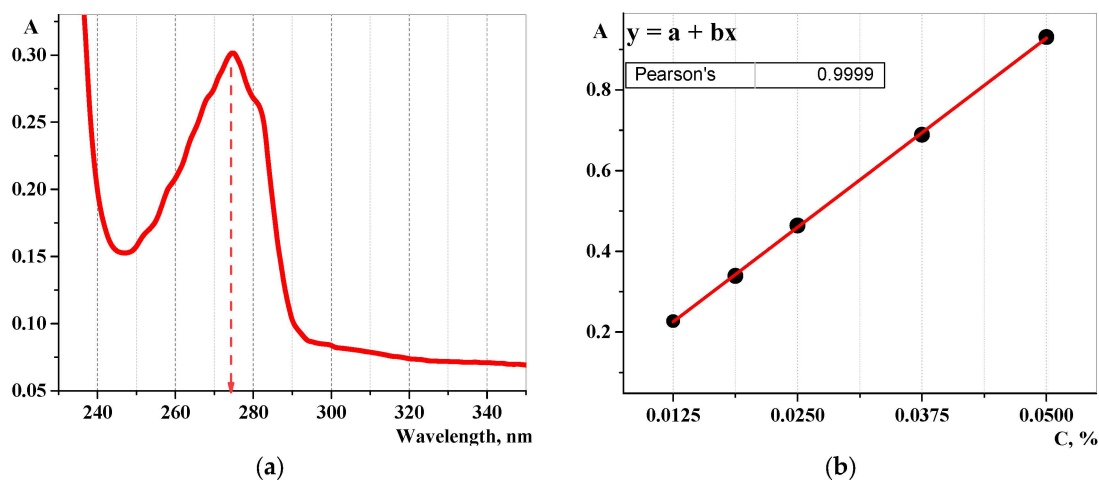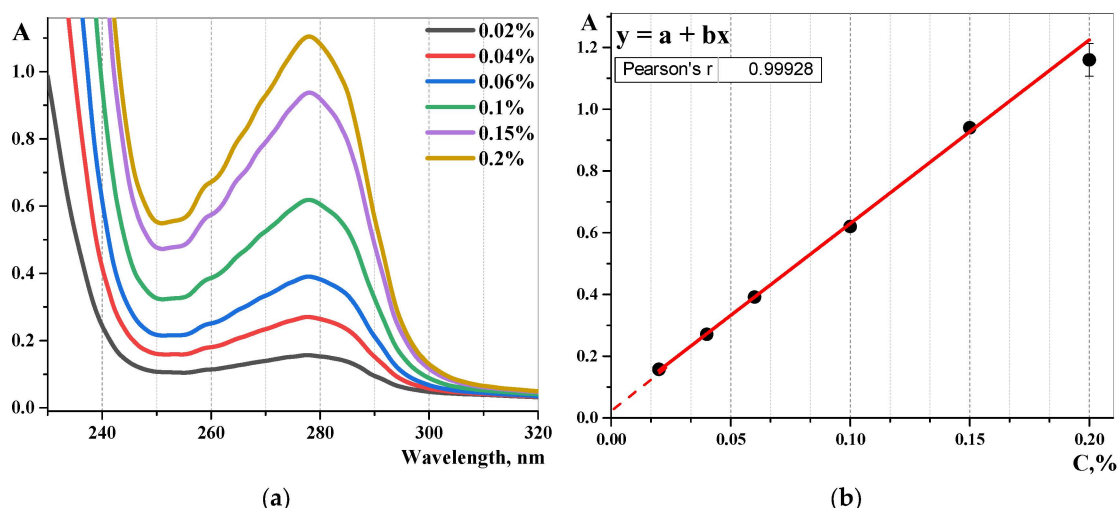

Figure 4. Results of DMTP electron spectroscopy (UV): (**a**) absorption spectrum of 0.023% DMTP; (**b**) calibration lines for DMTP assay (n = 3, p = 0.95).

The absorption spectrum of the 0.023% solution is characterized by λ_{max} at 276 ± 2 nm and λ_{min} at 248 ± 2 nm, which may provide the basis for approaches to its qualitative analysis (see Figure 4a). Meanwhile, the concentration dependence over a linear range of DMTP concentrations from 0.0125% to 0.0500% can be used to quantitatively DMTP analysis (see Figure 4b).

Bovine serum albumin (BSA) is known to be used as a standard in various protein quantification methods, which may be appropriate for the determination of DMTP in the absence of available comparison and CRS samples (Figure 5).

Figure 5. Results of BSA electron spectroscopy: (**a**) absorption UV spectrum; (**b**) calibration lines for protein assay (*n* = 3, *p* = 0.95).

As can be seen from the presented Figures 4 and 5, the DMTP spectrum corresponds to the BSA in terms of position and height of the absorption maximum (at the same concentrations). This fact indicates the possibility of determining DMTP by spectrum and calibration dependence for BSA in the absence of dermorphine CRS samples.

The results of the electronic spectroscopy method facilitated the computation of the specific absorption coefficient $E_{1\,cm}^{1\%}$ for aqueous solutions in a linear concentration range from 0.0125% to 0.0500%, aiding in the DMTP identification (Table 2).

Table 2. UV spectrophotometric analysis results in dermorphin tetrapeptide for qualitative and quantitative analysis.

C, %	A λ_{max} = 275 nm	$E_{1cm}^{1\%}$ (100 mL·g^{-1}·cm^{-1})
0.0125	0.227	18.20
0.0188	0.339	18.10
0.0250	0.464	18.60
0.0375	0.689	18.40
0.0500	0.931	18.60
		$\overline{E_{1cm}^{1\%}}$ ± SD = 18.38 ± 0.23

The calculated specific extinction value of DMTP at 275 nm can be used to determine the content of the polypeptide in aqueous solutions of pharmaceuticals.

The least-squares method is used to determine the parameters of the absorption domain and the linear dependence between the absorbance (A) and concentration, ranging from 0.0125% to 0.0500%, which may serve as quantitative analysis of DMTP solutions by the calibration graph method (Table 3).

Table 3. Validation parameters for linearity of UV results in the analytical range of DMTP solutions.

Parameters of Linear Dependence			y = a + b · x	
Constant (Free) Term, a ± SD	Slope, b ± SD	Coefficient of Determination, (R-Square)	Adjusted R^2	Pearson's Coefficient, r
−0.0087 ± 0.005	18.74 ± 0.16	0.9998	0.9997	0.9999
	y = −0.0087 + 18.74 · x			

3.1.3. Determination of Elemental Composition

Using energy-dispersive X-ray analysis, 11 elements were detected in the DMTP sample, many of which are essential: Al, Ca, Cl, Cu, Co, Fe, K, Mn, S, Si, and Zn (Figure 6) [29,30]. It is known that many factors influence the height of X-ray peaks, related to the nature of the sample, the system used for generating X-rays, and the detector used for measuring the X-ray spectrum. Mylar of appropriate thickness was used as the absorbing material film, which does not produce undesirable secondary X-rays [31]. However, even adhering to the specified experimental conditions, the X-ray peak height is not always directly proportional to the element concentration in the sample. This is due to the ZAF matrix effect (Atomic number (Z), Absorption (A), and Fluorescence (F)), and because the peak height of an element is primarily proportional to its prevalence in the sample, rather than the apparent concentration [32].
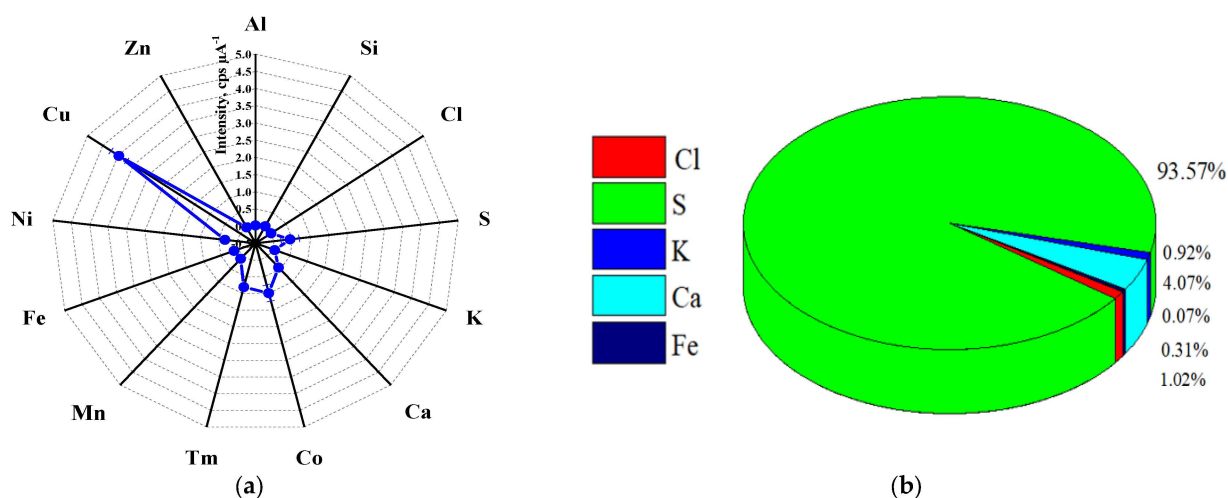
Figure 6. X−ray fluorescence detection of elements in dermorphin tetrapeptide sample in units of fluorescence intensity (**a**); and in units of concentration of the defined element (**b**).

The obtained spectrum profile shows that the elements copper (Cu) and cobalt (Co) have the highest X-ray emission intensities compared to other elements (see Figure 6a).

Matrix corrections to the initial intensities, considering the differences in composition between the DMTP sample and the standard, showed a concentration profile in the DMTP sample with a predominance of sulfur (S) (see Figure 6b).

3.2. Distributions of Particle Sizes

To analyze the dispersibility of aqueous and non-aqueous solutions, laser analysis methods were employed. These methods rely on the interaction of monochromatic, coherent, and narrowly directed beams of radiation with particles, their groups, or fluctuations, resulting in scattering.

3.2.1. Surface and Near-Surface Morphology

The SEM method was also used to describe the particle morphology. The studies were conducted in the mode of secondary electron registration at an accelerating voltage of 10 kV and a working distance of 15 mm at magnifications up to ×40,000 [33]. The results of electron-microscopic studies are presented in Figures 7 and S1.
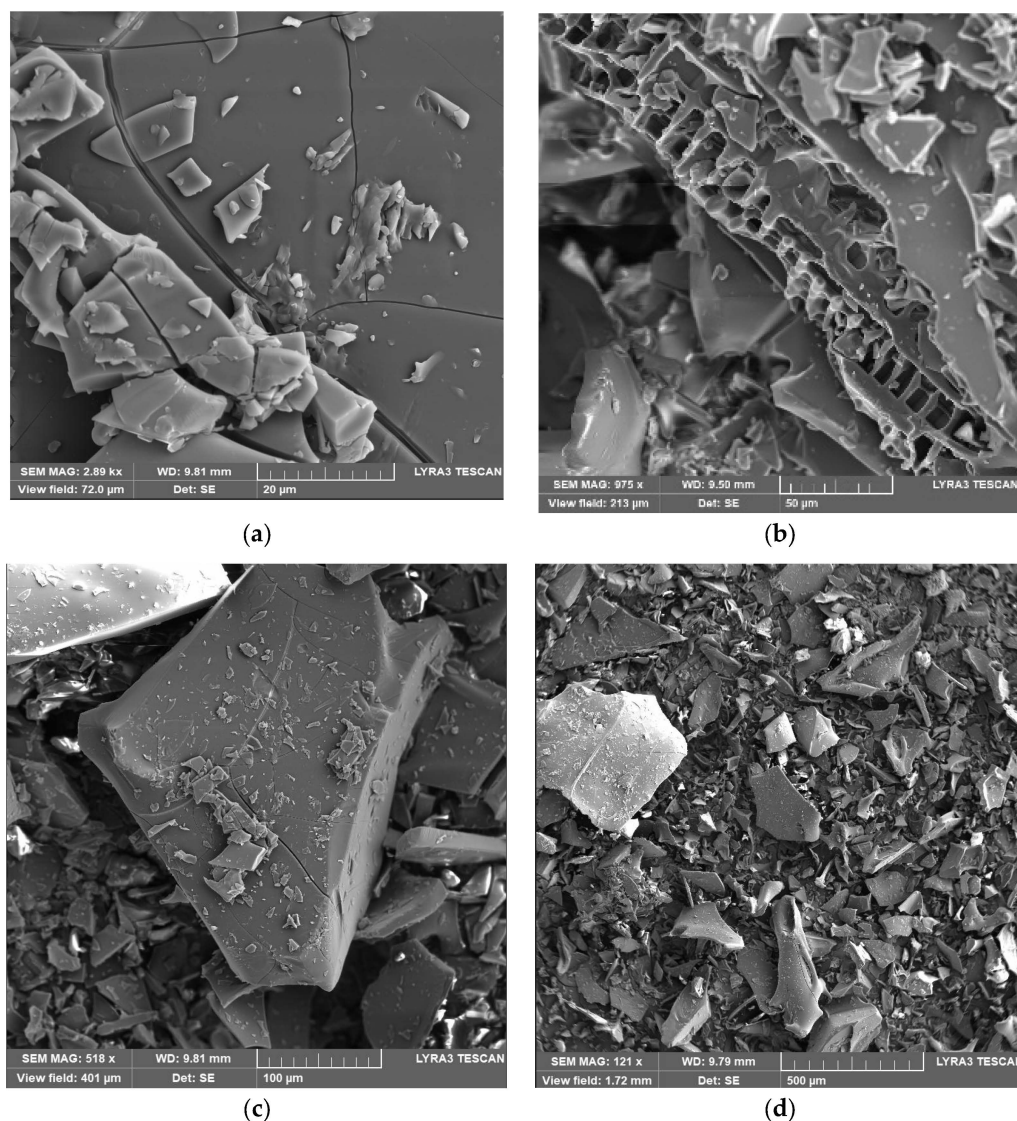
Figure 7. SEM micrographs for dermorphin tetrapeptide sample with different device magnification and scale bars (SB): (**a**) 2.89 k×, SB = 20 µm; (**b**) 975×, SB = 50 µm; (**c**) 518×, SB = 100 µm; (**d**) 121×, SB = 500 µm. MAG—Magnification = image pixel size/raster pixel size.

The particles of native dermorphin polypeptide are non-transparent, plank-shaped, large, and lamellar particles with a smooth surface, without additional inclusions, and with angular-shaped edges. Conglomerates and druzes covered with very fine particles occur (see Figure 7c); sizes range from 2 µm to 100 µm (see Figure 7a).

3.2.2. LALLS Study

The "size spectra" of the particle ensemble distribution in the heterogeneous solution of n-hexane in the range from 1 µm to 120 µm is presented (Figure 8). The complete characterization of the DMTP micron dispersion allows for the estimation of integral dispersion parameters: laser obscuration, volume concentration (%), and specific surface area (m^2/cm^3).
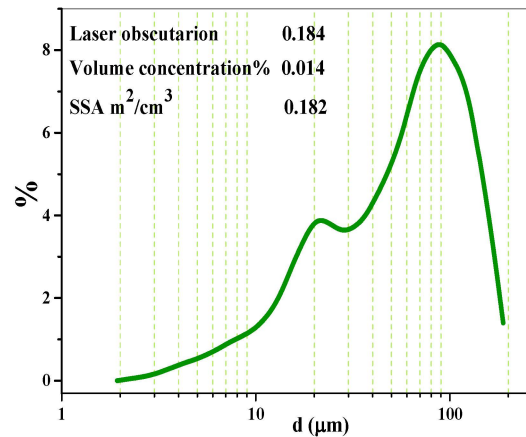
Figure 8. Dispersive properties of DMTP sample in *n*-hexane medium according to the LALLS method.

The results of the micron phase particle size analysis of tetrapeptide dermorphin in the *n*-hexane medium are presented in two size groups with distribution peaks at d = 20 μm and d = 90 μm; a significant portion of the solution volume is occupied by the size group at d = 90 μm with a specific surface area of 0.182 m^2/cm^3. The results of the static laser light scattering method may be of interest in the manufacture of pharmaceutical forms for external and internal *per os* application in the prediction of their bioavailability [34].

3.2.3. DLS Study

Dispersion properties of DMTP aqueous solution, in particular, their ability to form submicron particles that affect the biological activity and physical–chemical properties, were evaluated on the basis of an analysis of the autocorrelation function of the scattered light intensity fluctuations [35] (Figure 9).
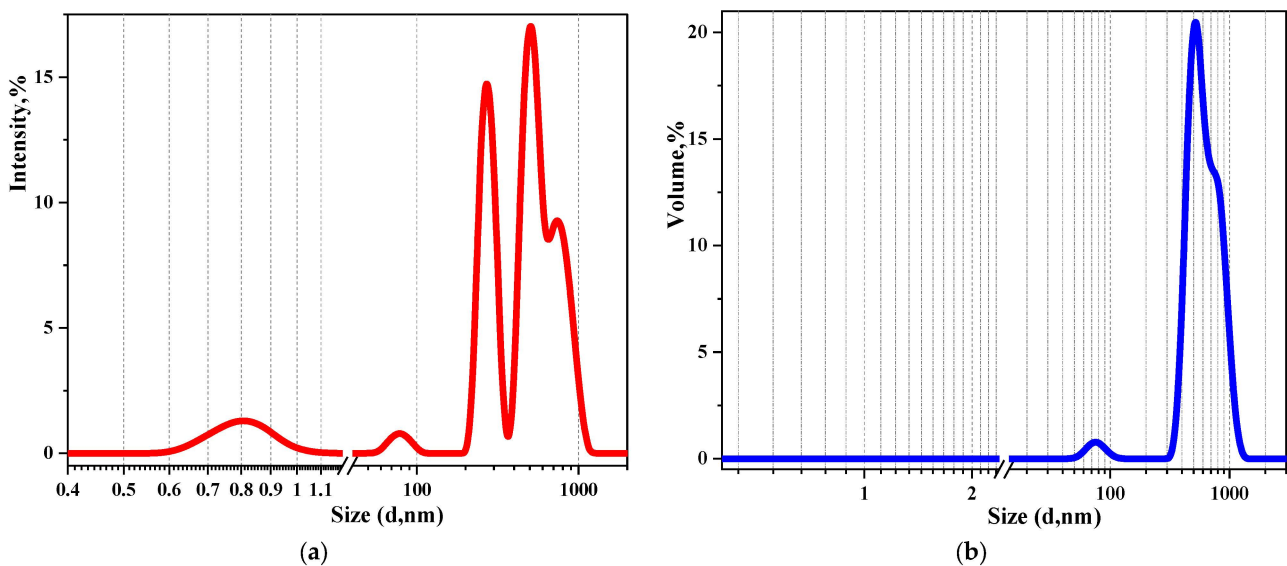

Figure 9. Dispersive properties of the aqueous 0.25% solution of DMTP according to particle size distribution: (**a**) in laser scattering intensity units; (**b**) in volumetric concentration units.

We observe a bimodal particle size distribution in the range of 300 nm to 500 nm, where the peaks are characterized by similar intensities. On the volumetric distribution graph, there is a prominent peak corresponding to particles with a size in the 500 nm range, occupying approximately 20% of the aqueous solution volume. The obtained data on the

size groups in the submicron range can be used to identify the API and to predict the properties of polypeptide solutions.

3.3. Optical Activities Study

There are several asymmetric carbon atoms in the structure of dermorphin, so the DMTP exists as enantiomers and diastereomers. We have recorded optical activity and obtained a very high correlation between the angle of rotation and the concentration of aqueous solutions of DMTP (Figure 10).
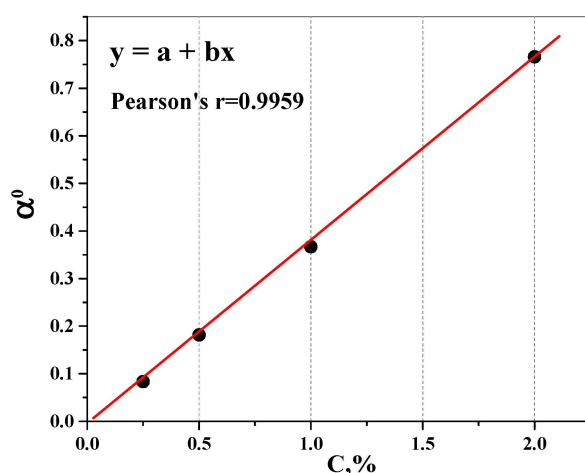
Figure 10. The dependence of the optical rotation angle on the concentration of DMTP aqueous solutions ($n = 3$, $p = 0.95$).

The optical activity of DMTP aqueous solutions in the concentration range from 0.25% to 2.00% is represented by the right-hand rotation of the plane of polarized light. The specific optical rotation depends on the nature of the substance and is equal to $[\alpha]_D^{20} = + 36.18 \pm 2.04$ [$°·mL·g^{-1}·dm^{-1}$], according to Biot's Law [36]. This direct dependence between α and the percentage concentration allows for the use of polarimetric analysis for quality-control purposes, such as determining the «identification» and «chiral purity» tests of dermorphin tetrapeptides, as well as their «assay».

3.4. In Silico and In Vivo (Biotesting) Analysis

3.4.1. Molecular Docking Technique

The most favorable orientations and conformations of the low-molecular-weight ligand DMTP in the active binding site with MOR are presented for the formation of a supramolecular complex visualized in PyMol [37] (Figure 11).

The contact area of the low-molecular-weight opioid ligand DMTP with the structure of the μ-opioid receptor 8E0G involves the key amino acid residue arginine (Arg 182) [38]. We can see the bond between the C=O group of tyrosyl and arginyl amino acid of 1.9 angstroms long. The complexity of molecular docking is further compounded when dealing with peptide structures, characterized by a multitude of rotating degrees of freedom. This inherent flexibility presents challenges in accurately predicting the binding interactions between the peptide and its receptor. Moreover, it is plausible that the peptide structure may undergo conformational changes prior to binding with the receptor, a phenomenon that remains poorly understood.
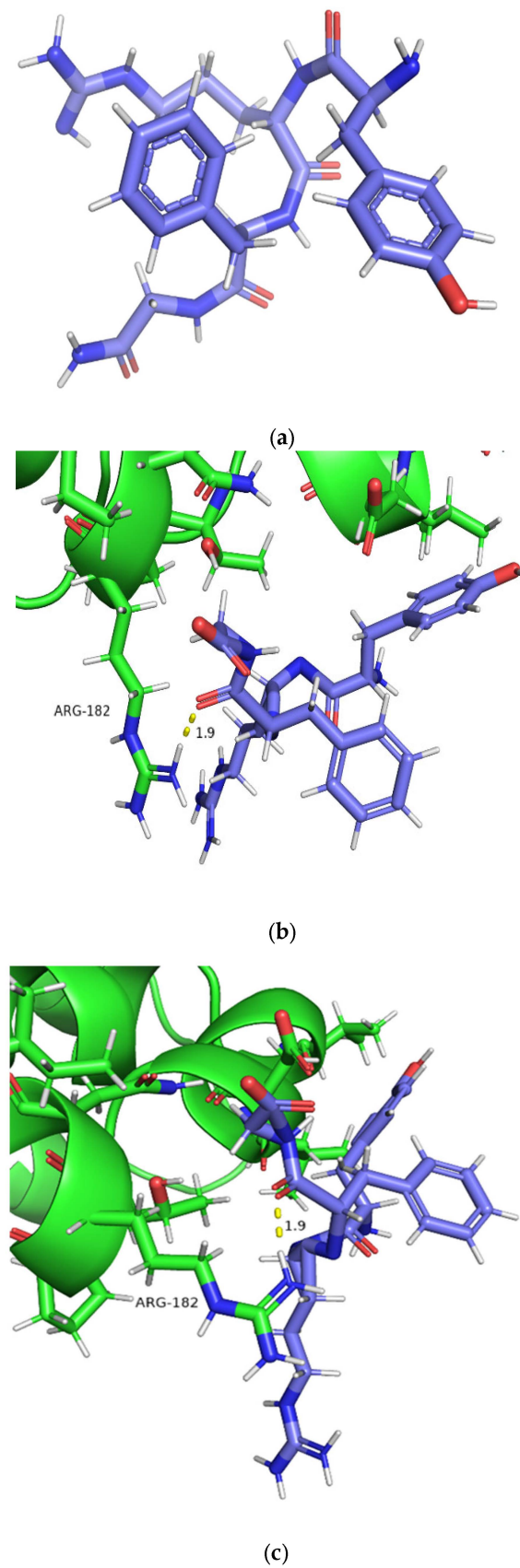
Figure 11. Modeling on the docked adducts example: (**a**) fixed spatial (3D) structure for DMTP, constructed in PyMol; (**b**,**c**) docking conformation obtained for DMTP with specific regions of MOR target protein (with distances in Å) in different imaging planes. Hydrogen bonds are depicted as yellow lines; for clarity, non-polar hydrogen atoms have been omitted.

These potential structural alterations add another layer of complexity to the docking process, underscoring the need for comprehensive investigations to understand the dynamic behavior of peptides and their implications for receptor binding. Further docking studies will improve prediction accuracy [39].

3.4.2. Spirotox Biotesting

To demonstrate the biological effect of the DMTP polypeptide on the test culture *Sp. ambiguum,* the apparent activation energy of the cell transition to the dead state, which is the rate-determining step, was evaluated (see Scheme 1). From a kinetic point of view, the low-molecular-weight ligand effectively catalyzes the death process, accelerating it to laboratory-recordable times (Tables S1–S3). Therefore, it can be assumed that the parameter $^{obsc}E_a$ (kJ/mol) serves as a quantitative criterion for the biological activity/toxicity of the ligand. The graphical dependence in coordinates «lifetime t_L,s − T, K» is presented in Figure 12.
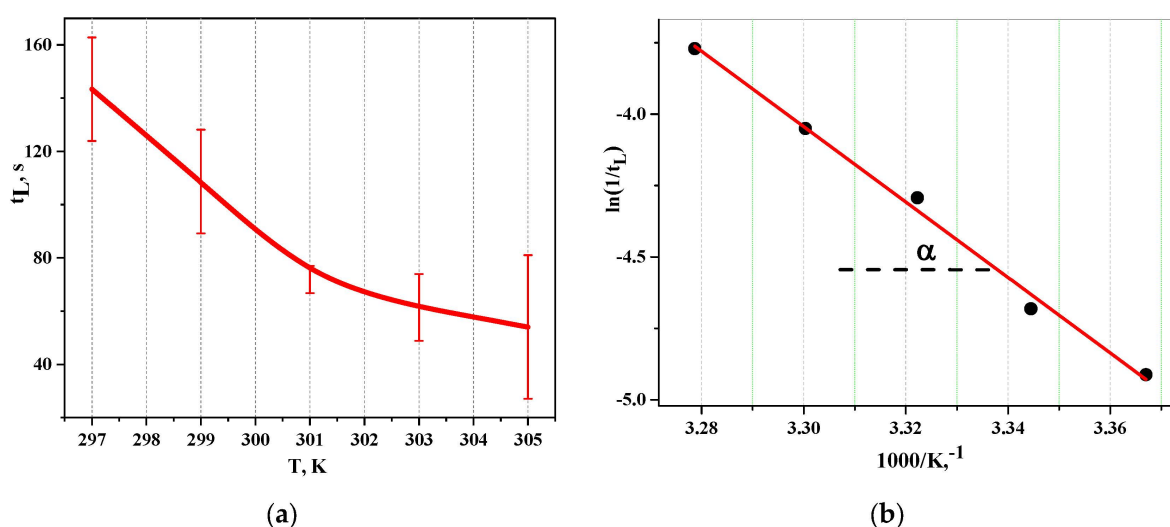
Figure 12. Relationship of *S. ambigua* lifetime as a function of temperature for the samples of 0.1% DMTP water solutions (pH = 5.47 ± 0.01): (**a**) in direct coordinates; (**b**) in Arrhenius coordinates.

Linearization in Arrhenius coordinates $\ln(1/t_L) = f(1/T)$ (Equation (3), Figure 12b) allowed for the calculation of the apparent (obseved) activation energy: $^{obsc}E_a = 111.5 \pm 15.9$ kJ/mol:

$$Ea = -R \cdot \text{tg}\alpha \tag{3}$$

where R—is the universal gas constant (8.31 J/mol·K); tgα—is the tangent of α angel.

The two-dimensional diagram in the coordinates "$^{obsc}Ea - LD_{50}$" that we compiled earlier [40], based on the Spirotox study and literature data on LD_{50} (rats, *per os*), will allow to predict of drug toxicity by extrapolation to the OX axis (Figure 13).

According to the diagram, the aqueous solution of the tested DMTP polypeptide occupies an intermediate position between the toxicity of trichloroacetic acid, hawthorn tincture (dilution 1:4), phenol, and motherwort tincture (dilution 1:10).
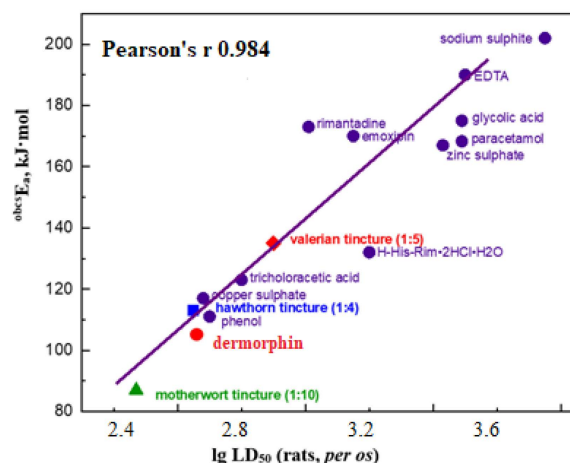
Figure 13. Diagram "$^{obcs}E_a - LD_{50}$" of mutual correspondence between values of apparent activation energy of biosensor cell death process activation in media of different xenobiotics and median lethal dose for laboratory rats.

4. Conclusions

An integrated approach, combining molecular docking software tools with spectroscopic, laser dispersive, microscopic, optical, and biological analytical methods, has allowed a thorough characterization of a representative of a promising class of peptide-based non-narcotic analgesics. The results obtained are crucial for strengthening pharmaceutical quality control in the production of dermorphin tetrapeptide preparations, ensuring higher efficacy and safety of their therapeutic use.

Abbreviations

ASIC	Acid-sensing ion channels
API	Active pharmaceutical ingredient
Arg	Arginin
ASIC	Acid-sensing ion channels
ATR	Attenuated total reflectance
BAS	Bioactive substances
BSA	Bovine serum albumin
CNS	Central nervous system
CRS	Chemical reference substance
DLS	Dynamic light scattering
DMTP	Dermorphin tetrapeptide
$^{obs}E_a$	Activation energy (observed)
FTIR	Fourier-Transform IR Spectroscopy
IPT	Intramolecular proton transfer
OM	Optical microscopy
LALLS	Low-angle Laser Light Scattering
MAG	Magnification
MOR	μ-opioid receptor
Mus musculus	House mouse
CNS	Central nervous system
PDB	Protein data bank
PdI	Polydispersity index
PNS	Peripheral nervous system
SEM	Scanning electron microscopy
SLS	Static Light Scattering
SSA	Specific Surface Area
Spirotox test	*Spirostomum ambiguum* acute toxicity test
VC	Volumetric concentration
UV	Ultraviolet
XRF	X-ray fluorescence

References

1. Corder, G.; Castro, D.C.; Bruchas, M.R.; Scherrer, G. Endogenous and Exogenous Opioids in Pain. *Annu. Rev. Neurosci.* **2018**, *41*, 453–473. [CrossRef] [PubMed]
2. Hochrainer, N.; Serafin, P.; D'Ingiullo, S.; Mollica, A.; Granica, S.; Brytan, M.; Kleczkowska, P.; Spetea, M. In Vitro and In Vivo Pharmacological Profiles of LENART01, a Dermorphin-Ranatensin Hybrid Peptide. *Int. J. Mol. Sci.* **2024**, *25*, 4007. [CrossRef] [PubMed]
3. Paul, A.K.; Smith, C.M.; Rahmatullah, M.; Nissapatorn, V.; Wilairatana, P.; Spetea, M.; Gueven, N.; Dietis, N. Opioid Analgesia and Opioid-Induced Adverse Effects: A Review. *Pharmaceuticals* **2021**, *14*, 1091. [CrossRef] [PubMed]
4. Benyamin, R.; Trescot, A.M.; Datta, S.; Buenaventura, R.; Adlaka, R.; Sehgal, N.; Glaser, S.E.; Vallejo, R. Opioid complications and side effects. *Pain Physician* **2008**, *11*, S105–S120. [CrossRef]
5. Montecucchi, P.C.; de Castiglione, R.; Piani, S.; Gozzini, L.; Erspamer, V. Amino acid composition and sequence of dermorphin, a novel opiate-like peptide from the skin of *Phyllomedusa sauvagei*. *Int. J. Protein Res.* **1981**, *17*, 275–283. [CrossRef]
6. Malpezzi-Marinho, E.L.A.; Zanoni, C.I.S.; Molska, G.R.; Paraventi, C.; Wuo-Silva, R.; Berro, L.F.; Parada, C.A.; Tamura, E.K.; Marinho, E.A.V. Antinociceptive Activity of the Skin Secretion of *Phyllomedusa rohdei* (Amphibia, Anura). *Toxins* **2020**, *12*, 589. [CrossRef]
7. Lacombe, C.; Cifuentes-Diaz, C.; Dunia, I.; Auber-Thomay, M.; Nicolas, P.; Amiche, M. Peptide secretion in the cutaneous glands of South American tree frog *Phyllomedusa bicolor*: An Ultrastructural study. *Eur. J. Cell Biol. Suppl.* **2000**, *79*, 631–641. [CrossRef]
8. Delfino, G.; Alvarez, B.B.; Brizzi, R.; Cespedez, J.A. Serous cutaneous glands of Argentine *Phyllomedusa* wagler 1830 (Anura Hylidae): Secretory polymorphism and adaptive plasticity. *Trop. Zool.* **1998**, *11*, 333–351. [CrossRef]
9. Melchiorri, P.; Negri, L. The dermorphin peptide family. *Gen. Pharmacol.* **1996**, *27*, 1099–1107. [CrossRef]

10. Mizoguchi, H.; Bagetta, G.; Sakurada, T.; Sakurada, S. Dermorphin tetrapeptide analogs as potent and long-lasting analgesics with pharmacological profiles distinct from morphine. *Peptides* **2011**, *32*, 421–427. [CrossRef]

11. Kosorukov, V.S.; Abuzarova, G.R.; Zakharochkina, E.R.; Gamzeleva, O.Y.; Yatsenko, K.A. Tafalgin is a Russian innovative tetrapeptide pharmaceutical for subcutaneous injection: Review of the results of phase I and II clinical trials. *Head Neck Tumors HNT* **2022**, *12*, 89–107. [CrossRef]

12. Stein, C.; Schäfer, M.; Machelska, H. Attacking pain at its source: New perspectives on opioids. *Nat. Med.* **2003**, *9*, 1003–1008. [CrossRef] [PubMed]

13. Abuzarova, G.R.; Sarmanayeva, R.R.; Alekseeva, G.S.; Brazhnicova, Y.V. A clinical case of the use of a new selective μ1-opioid analgesic Tafalgin in the treatment of chronic cancer pain. *J. Mod. Oncol.* **2022**, *24*, 313–318. [CrossRef]

14. Osmakov, D.I.; Onoprienko, L.V.; Kalinovskii, A.P.; Koshelev, S.G.; Stepanenko, V.N.; Andreev, Y.A.; Kozlov, S.A. Opioid Analgesic as a Positive Allosteric Modulator of Acid-Sensing Ion Channels. *Int. J. Mol. Sci.* **2024**, *25*, 1413. [CrossRef] [PubMed]

15. National Library of Medicine (US). Available online: https://pubchem.ncbi.nlm.nih.gov/compound/Tyrosyl-arginyl-phenylalanyl-glycinamide (accessed on 20 May 2024).

16. Makarova, M.P.; Syroeshkin, A.V.; Maksimova, T.V.; Matveeva, I.S.; Pleteneva, T.V. Features of Microelements Express-determination in Medicinal and Nonoficinal Plants by X-Ray-Fluorescence Analysis. *Drug. Dev. Regist.* **2019**, *8*, 93–97. (In Russian) [CrossRef]

17. Uspenskaya, E.V.; Kuzmina, E.; Quynh, H.T.N.; Komkova, M.A.; Kazimova, I.V.; Timofeev, A.A. Influence of Mechanical Loading on the Process of Tribochemical Action on Physicochemical and Biopharmaceutical Properties of Substances, Using Lacosamide as an Example: From Micronisation to Mechanical Activation. *Pharmaceutics* **2024**, *16*, 798. [CrossRef]

18. Morris, G.M.; Huey, R.; Lindstrom, W.; Sanner, M.F.; Belew, R.K.; Goodsell, D.S.; Olson, A.J. AutoDock4 and AutoDockTools4: Automated docking with selective receptor flexibility. *J. Comput. Chem.* **2009**, *30*, 2785–2791. [CrossRef]

19. Alam, N.; Goldstein, O.; Xia, B.; Porter, K.A.; Kozakov, D.; Schueler-Furman, O. High-resolution global peptide-protein docking using fragments-based Piper-FlexPepDock. *PLoS Comput. Biol.* **2017**, *13*, e1005905. [CrossRef]

20. London, N.; Raveh, B.; Cohen, E.; Fathi, G.; Schueler-Furman, O. Rosetta FlexPepDock web server—High resolution modeling of peptide–protein interactions. *Nucleic Acids Res.* **2011**, *39*, W249–W253. [CrossRef]

21. Neale, V.; Sotillo, J.; Seymour, J.; Wilson, D. The venom of the spine-bellied sea snake (*Hydrophis curtus*): Proteome, toxin diversity and intraspecific variation. *Int. J. Mol. Sci.* **2017**, *18*, 2695. [CrossRef]

22. Zamyatnin, A.A. Fragmentomics of natural peptide structures. *Biochemistry* **2009**, *74*, 1575–1585. [CrossRef] [PubMed]

23. Zamyatnin, A.A. Fragmentomics of proteins and natural oligopeptides. *Biophysics* **2008**, *53*, 329–335. [CrossRef]

24. Zhang, Y.; Ding, C.; Pan, L.; Cai, Y. Correlation of Intensity Fluctuations for Scattering of a Partially Coherent Plane-Wave Pulse. *Appl. Sci.* **2019**, *9*, 244. [CrossRef]

25. Warren, J.P.; Culbert, M.P.; Miles, D.E.; Maude, S.; Wilcox, R.K.; Beales, P.A. Controlling the Self-Assembly and Material Properties of β-Sheet Peptide Hydrogels by Modulating Intermolecular Interactions. *Gels* **2023**, *9*, 441. [CrossRef]

26. Cotabarren, J.; Tellechea, M.E.; Tanco, S.M.; Lorenzo, J.; Garcia-Pardo, J.; Avilés, F.X.; Obregón, W.D. Biochemical and MALDI-TOF Mass Spectrometric Characterization of a Novel Native and Recombinant Cystine Knot Miniprotein from *Solanum tuberosum* subsp. *andigenum* cv. Churqueña. *Int. J. Mol. Sci.* **2018**, *19*, 678. [CrossRef]

27. Ray, D.; Pramanik, A.; Guchhait, N. Lactim–lactam tautomerism through four member hydrogen bonded network in isoindole-fused imidazole system: A combined spectroscopic and theoretical approach to photophysical properties. *J. Photochem. Photobiol. A* **2014**, *274*, 33–42. [CrossRef]

28. Prasad, S.; Mandal, I.; Singh, S.; Paul, A.; Mandal, B.; Venkatramani, R.; Swaminathan, R. Near UV-Visible electronic absorption originating from charged amino acids in a monomeric protein. *Chem. Sci.* **2017**, *8*, 5416–5433. [CrossRef]

29. Cholewińska, E.; Marzec, A.; Sołek, P.; Fotschki, B.; Listos, P.; Ognik, K.; Juśkiewicz, J. The Effect of Copper Nanoparticles and a Different Source of Dietary Fibre in the Diet on the Integrity of the Small Intestine in the Rat. *Nutrients* **2023**, *15*, 1588. [CrossRef]

30. Genchi, G.; Lauria, G.; Catalano, A.; Carocci, A.; Sinicropi, M.S. Prevalence of Cobalt in the Environment and Its Role in Biological Processes. *Biology* **2023**, *12*, 1335. [CrossRef]

31. Khatun, S.; Akter, A.N.; Monika, M.M.; Rahman, M.M. Ahasan Standardization of Mylar Absorber Thickness of the Si(Li) X-ray Detector. *J. Nucl. Part. Phys.* **2020**, *10*, 36–42. [CrossRef]

32. Lacinska, A.; Rushton, J.; Burgess, S.; Deady, E.A.; Turner, G. The Effect of X-ray Energy Overlaps on the Microanalysis of Chevkinite (Ce, La, Ca, Th)$_4$(Fe^{2+}, Mg)$_2$(Ti, Fe^{3+})$_3$Si$_4$O$_{22}$ Using SEM EDS-WDS. *Minerals* **2021**, *11*, 1063. [CrossRef]

33. Ali, A.; Zhang, N.; Santos, R.M. Mineral Characterization Using Scanning Electron Microscopy (SEM): A review of the fundamentals, advancements, and research directions. *Appl. Sci.* **2023**, *13*, 12600. [CrossRef]

34. Gross-Rother, J.; Blech, M.; Preis, E.; Bakowsky, U.; Garidel, P. Particle detection and characterization for biopharmaceutical applications: Current principles of established and alternative techniques. *Pharmaceutics* **2020**, *12*, 1112. [CrossRef]

35. Shayeganfar, F.; Jabbari-Farouji, S.; Movahed, M.S.; Jafari, G.R.; Tabar, M.R. Multifractal analysis of light scattering-intensity fluctuations. *Phys. Rev. Stat. Nonlin. Soft Matter Phys.* **2009**, *80*, 061126. [CrossRef]

36. Leclercq, F. Arago, Biot, and Fresnel Elucidate Circular Polarization. *Rev. Hist. Sci.* **2013**, *66*, 395–416. [CrossRef]
37. Stetz, G.; Verkhivker, G.M. Dancing through Life: Molecular Dynamics Simulations and Network-Centric Modeling of Allosteric Mechanisms in Hsp70 and Hsp110 Chaperone Proteins. *PLoS ONE* **2015**, *10*, e0143752. [CrossRef]
38. Harms, M.J.; Schlessman, J.L.; Sue, G.R.; García-Moreno, B. Arginine residues at internal positions in a protein are always charged. *Proc. Natl. Acad. Sci. USA* **2011**, *108*, 18954–18959. [CrossRef]
39. Agu, P.C.; Afiukwa, C.A.; Orji, O.U.; Ezeh, E.M.; Ofoke, I.H.; Ogbu, C.O.; Ugwuja, E.I.; Aja, P.M. Molecular docking as a tool for the discovery of molecular targets of nutraceuticals in diseases management. *Sci. Rep.* **2023**, *13*, 13398. [CrossRef]
40. Pleteneva, T.V.; Galkina, D.A.; Fatkulina, O.A.; Ogotoeva, D.D.; Levitskaya, O.V.; Uspenskaya, E.V.; Syroeshkin, A.V. Arrhenius kinetics in the evaluation of the biological activity of pharmaceutical tinctures. *Int. J. Appl. Pharm.* **2023**, *15*, 277–281. [CrossRef]